Enhanced Photoluminescence from Si Nano-organosols by Functionalization with Alkenes and Their Size Evolution

Shu-Man Liu, Yang Yang, Seiichi Sato, and Keisaku Kimura*

Graduate School of Material Science, University of Hyogo, 3-2-1, Koto, Kamigori-cho, Ako-gun, Hyogo 678-1297, Japan

Received August 31, 2005. Revised Manuscript Received November 6, 2005

Silicon nanoparticles ranging from 2 to 16 nm were synthesized by a facile wet chemical route, in which SiO amorphous powder was annealed at 1000 °C, etched in hydrofluoric acid, and surface modified by alkene. After alkyl-termination of the particle surfaces, size selective precipitation technique was applied to separate the nanoparticles into uniform sized fractions. Transmission electron microscopy showed well-dispersed and highly crystalline silicon nanoparticles after the treatment by alkene. Visible room-temperature photoluminescence in the range 800−500 nm was observed from these nanoparticles. The photoluminescence intensity has significantly been enhanced by the surface functionalization. Moreover, the PL peak energy of the size-selected nanoparticles shifted to blue as the size decreased due to quantum confinement effect. The experimental result was also compared with the theoretical predictions and was found to follow the general trend of the model calculations.

Introduction

Since the discovery of red light emission upon UV excitation of porous silicon (PS) by Canham,[1] a great deal of research has focused on preparing nanosized silicon with visible photoluminescence (PL) as Si nanostructures have the potential to be integrated within existing silicon technology over other semiconductor nanocrystals. Due to the relative easiness of producing PS by etching silicon wafers, there have been many studies of optical properties of PS, but low efficiency and instability of the photoluminescence from PS inhibit their further fundamental investigation and commercial applications. The PL intensity of PS is mainly limited by nonradiative carrier recombination on defects produced during the etching process,[2] and the poor PL stability of PS is mainly owing to the generation of nonradiative defects at the initially hydrogen-terminated nanocrystalline Si surface upon oxidation during storage in air. To enhance the PL intensity of PS, some oxidation techniques such as electrochemical or thermal processing have been attempted.[3−8] Meanwhile, to enhance the red-band luminescence stability, many groups have carried out chemical modifications of the PS surface to replace the initial metastable Si−H bonds on nanocrystalline Si surfaces by stable covalent Si−C bonds. For instance, Buriak and co-workers reported on surface functionalization of PS with alkenes and alkynes through Lewis acid-mediated or white light-promoted reactions.[9−11] Bateman et al. presented the covalent modification of PS by direct reaction with unsaturated hydrocarbons in the absence of catalyst.[12] Boukherroub et al. modified PS surfaces with ethyl undecylenate to achieve greatly enhanced PL.[13] They also linked activated esters of undecylenic acid covalently to a PS surface via a thermal hydrosilylation reaction.[14] Surface functionalization of free-standing Si nanoparticles produced by solution route has also been explored recently. Korgel and co-workers developed a new method to produce octanol-capped Si nanocrystals at a supercritical high pressure and temperature and showed PL emission near UV and green region.[15] They also investigated the PL of single Si particles in the visible range from green to red.[16] Kauzlarich and co-workers have reported a series of papers[17−23] on synthesis of alkyl-capped Si nanoparticles by a solution route at room temperature in anaerobic and

* To whom correspondence should be addressed. E-mail: kimura@sci.u-hyogo.ac.jp. Tel: 81-791-58-0159. Fax: 81-791-58-0161.

(1) Canham, L. T. *Appl. Phys. Lett.* **1990**, *57*, 1046.
(2) (a) Cullis, A. G.; Canham, L. T.; Calcott, P. D. J. *J. Appl. Phys.* **1997**, *82*, 909. (b) Kimura, K. *J. Appl. Phys.* **1998**, *83*, 1345.
(3) Prokes, S. M. *Appl. Phys. Lett.* **1993**, *62*, 3244.
(4) Yamani, Z.; Ashhab, S.; Nayfeh, A.; Thompson, W. H.; Nayfeh, M. *J. Appl. Phys* **1998**, *83*, 3929.
(5) Gelloz, B.; Nakagawa, T.; Koshida, N. *Appl. Phys. Lett.* **1998**, *73*, 2021.
(6) Belomoin, G.; Therrien, J.; Nayfeh, M. *Appl. Phys. Lett.* **2000**, *77*, 779.
(7) Kovalev, D.; Gross, E.; Diener, J.; Timoshenko, V. Yu.; Fujii, M. *Appl. Phys. Lett.* **2004**, *85*, 3590.
(8) Gelloz, B.; Kojima, A.; Koshida, N. *Appl. Phys. Lett.* **2005**, *87*, 31107.
(9) Buriak, J. M.; Allen, M. J. *J. Am. Chem. Soc.* **1998**, *120*, 1339.
(10) Buriak, J. M.; Stewart, M. P.; Geders, T. W.; Allen, M. J.; Choi, H. C.; Smith, J.; Raftery, D.; Canham, L. T. *J. Am. Chem. Soc.* **1999**, *121*, 11491.
(11) Stewart, M. P.; Buriak, J. M. *J. Am. Chem. Soc.* **2001**, *123*, 7821.
(12) Bateman, J. E.; Eagling, R. D.; Worrall, D. R.; Horrocks, B. R.; Houlton A. *Angew. Chem., Int. Ed.* **1998**, *37*, 2683.
(13) Boukherroub, R.; Wayner, D. D. M.; Sproule, G. I.; Lockwood, D. J.; Canham, L. T. *Nano Lett.* **2001**, *1*, 713.
(14) Wojtyk, J. T. C.; Morin, K. A.; Boukherroub, R.; Wayner, D. D. M. *Langmuir* **2002**, *18*, 6081.
(15) Holmes, J. D.; Ziegler, K. J.; Doty, R. C.; Pell, L. E.; Johnston, K. P.; Korgel, B. A. *J. Am. Chem. Soc.* **2001**, *123*, 3743.
(16) English, D. S.; Pell, L. E.; Yu, Z. Barbara, P. F.; Korgel, B. A. *Nano Lett.* **2002**, *2*, 681.
(17) Yang, C.; Bley, R. A.; Kauzlarich, S. M.; Lee, H. W. H.; Delgado, G. R. *J. Am. Chem. Soc.* **1999**, *121*, 5191.
(18) Baldwin, R. K.; Pettigrew, K. A.; Ratai, E.; Augustine, M. P. *Chem. Commun.* **2002**, 1822.
(19) Baldwin, R. K.; Pettigrew, K. A.; Garno, J. C.; Power, P. P.; Liu, G. Y.; Kauzlarich, S. M. *J. Am. Chem.* Soc. **2002**, *124*, 1150.
(20) Bley, R. A.; Kauzlarich, S. M. *J. Am. Chem. Soc.* **1996**, *118*, 12461.

10.1021/cm0519636 CCC: $33.50
Published on Web 01/13/2006

anhydrous conditions through the reduction of silicon tetrahalides and other alkylsilicon halides, or oxidation of metal silicide. Blue−UV PL emissions were observed from some of their samples. More recently, Swihart and co-workers developed a new combined vapor-phase and solution-phase process. Large-scale Si nanoparticles were prepared by CO_2 laser-induced pyrolysis of silane, and the particles exhibited bright PL after etching with mixtures of hydrofluoric acid (HF) and nitric acid (HNO_3).[24] They also presented surface functionalization of their Si nanoparticles with several organic reagents, which increased the stability of the PL substantially.[25−27] Although there have been some papers published on synthesis of Si nanocrystals and their surface functionalization by several solution routes as described above, there is less experimental agreement on the photoluminescence energies of Si nanoparticles even with similar size range and surface termination. Moreover, understanding of the luminescence behavior of these Si nanoparticles is rather complicated and still far from complete. Further studies on high-quality samples, particularly the photophysics of samples with narrow size distributions, are needed since chemically stable, uniform-sized, and well-dispersed Si nanoparticles with well-defined and controllable optical properties are of great benefit for further application as tags for biologically sensitive materials and in optoelectronics.

Recently, a low-cost and simple route has been developed for large-scale synthesis of Si nanopowders in our group, in which commercially available amorphous SiO_x ($x < 2$) powder was annealed at high temperature and then etched by HF solution.[28] The hydrogen-capped Si nanoparticles with little oxide present prepared by carefully controlling the etching condition could be redispersed in several organic solvents. In this work, we report the surface modification of the HF-etched Si nanoparticles through the thermal reaction with alkene reagent in organic solution. This route can enhance not only the stability of organic dispersions of Si nanoparticles but also the PL intensity even if the surfaces of HF-etched particles are not free of oxide. Size-selective precipitation technique was applied to the alkyl-capped Si particle dispersion to narrow the size distribution of the sample. As for optical properties, we focus on the photoluminescence of the well-dispersed Si nanoparticles during the thermal reaction and after size-selective precipitation.

Experimental Section

Materials. Silicon monooxide (SiO) powders (99.95%) were purchased from Nilaco Co. HF (46.0−48.0%), methanol (99.8%), toluene (99.5%), and L-octene (95%) were purchased from Wako Pure Chemicals without further purification. Distilled water was produced by an Advantec GS-200 automatic water-distillation supplier.

Preparation of Si Nanoparticles. Si nanoparticles were synthesized using a procedure described in detail previously[28] with small modification. Here, SiO powders were used as starting materials. In brief, SiO powders were annealed at high temperature of 1000 °C for 2 h under a flow of Ar gas at ambient atmosphere. Then annealed powders were suspended in water mixed with a small amount of methanol under mild ultrasonic treatment. To the suspension, an HF aqueous solution (5−10%) was added to dissolve the silicon dioxide in annealed powders. Typically, annealed powders of 200 mg were etched in HF solution (10%) for 1 h. Si particles were collected on polyvinylidene fluoride (PVDF) membrane filters (Millipore) from the suspensions. These HF-etched Si nanoparticles were washed with distilled water and methanol thoroughly to remove byproducts and excess HF and dried in a N_2 stream. Usually about 10% of the original powder mass (the price of which is almost comparable to that of Si wafer) is recovered after this etching process.

Surface Termination of Si Nanoparticles by Alkene. A thermal alkylation reaction of hydrogen-terminated surface of Si nanoparticles with alkene in the absence of catalyst similar to refs 12 and 25 was carried out. Toluene and 1-octene were bubbled with pure nitrogen before use to remove dissolved oxygen. In a typical process, HF-etched Si nanoparticles were dispersed in 100 mL of toluene, and 9 mL of 1-octene was added. The solution was sonicated for 30 min and then refluxed with stirring and N_2 bubbling at 110−150 °C for 3−48 h. During the reaction, a small portion of solution was taken at a certain interval for the PL measurement. After the reaction, the solution became clear bright yellow or orange. In some cases there remained a few dark brown powders at the bottom of the flask, which can be removed by centrifugation.

Size-Selective Precipitation of Alkyl-Capped Si Nanoparticles. The clear dispersion of Si nanoparticles was concentrated by evaporation of solvent, and then methanol was added dropwise. Once it changed to slightly cloudy, the dispersion was centrifugated at 12000 rpm for 15 min using a Kubota 1720 centrifuge to separate the solid sample containing mainly the larger particles, which was redispersed in toluene or other nonpolar organic solvent. This procedure was repeated several times for separation of particles with different average size.

Instruments. X-ray diffraction (XRD) measurements of annealed, etched, and alkyl-terminated Si particles were carried out on a Rigaku Rint 2000 diffractometer with Cu Kα radiation (λ = 1.5418 Å) operated at 40 kV and 20 mA. Fourier transform infrared (FTIR) spectra were measured with a Horiba FT-210 infrared spectrophotometer using a 150 mg KBr disk dispersed with the powder samples at a weight ratio of about 0.5%. Annealed powders and etched particles collected on membranes were used directly as powder samples for XRD and FTIR measurements. For alkyl-terminated particle dispersions, the solvent was evaporated at reduced pressure after refluxing, and the resulting oily solid was used for XRD and FTIR measurement. A Hitachi-8100 transmission electron microscope (TEM) operated at 200 kV was used to measure the size and analyze the structure of Si nanoparticles. The suspension was dropped on a carbon-coated Cu grid and dried in air. The histogram of the nanoparticles was obtained by measuring the diameters of particles with a NIH Image 1.30v software package. PL spectra were recorded with a Hitachi F-4500 fluorescence spectrophotometer at room temperature. The Si particle suspensions were excited by a 150 W xenon lamp. The excitation wavelength was selected at 350 nm and the emission cutoff filter was set to 420 nm for all the measurements shown hereafter.

(21) Mayeri, D.; Phillips, B. L.; Augustine, M. P.; Kauzlarich, S. M. *Chem. Mater.* **2001**, *13*, 765.
(22) Pettigrew, K. A.; Liu, Q.; Power, P. P.; Kauzlarich, S. M. *Chem. Mater.* **2003**, *15*, 4005.
(23) Zou, J.; Baldwin, R. K.; Pettigrew, K. A.; Kauzlarich, S. M. *Nano Lett.* **2004**, *4*, 1181.
(24) Li, X.; He, Y.; Talukdar, S. S.; Swihart, M. T. *Langmuir* **2003**, *19*, 8490.
(25) Li, X.; He, Y.; Swihart, M. T. *Langmuir* **2004**, *20*, 4720.
(26) Li, Z. F.; Swihart, M. T.; Ruckenstein, E. *Langmuir* **2004**, *20*, 1963.
(27) Hua, F.; Swihart, M. T.; Ruckenstein, E. *Langmuir* **2005**, *21*, 6054.
(28) Liu, S. M.; Sato, S.; Kimura, K. *Langmuir* **2005**, *21*, 6324.

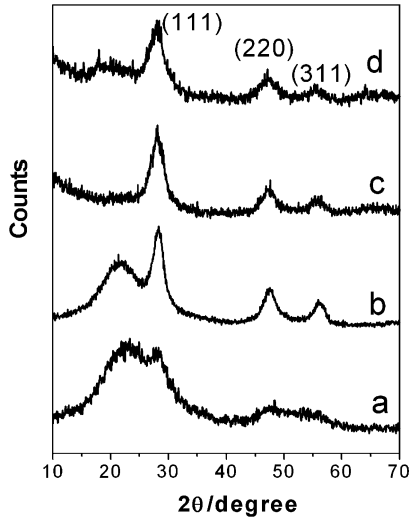

Figure 1. XRD patterns of (a) SiO powder, (b) 1000 °C annealed powder, (c) HF-etched sample, and (d) octene-treated sample.

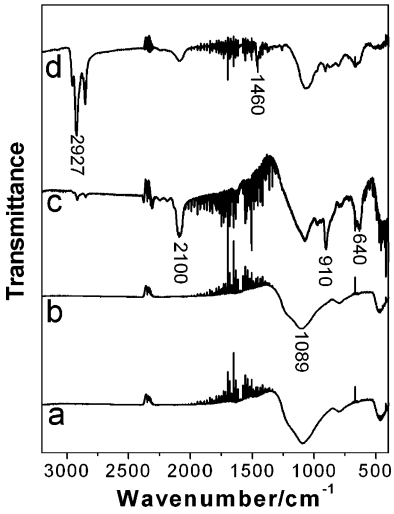

Figure 2. FTIR spectra of (a) SiO powder, (b) 1000 °C annealed powder, (c) HF-etched sample, and (d) octene-treated sample.

Results and Discussion

Preparation and Structural Characterization. Si nanocrystallites were formed from amorphous SiO starting materials during annealing at 1000 °C according to the following reaction:

$$2\mathrm{SiO} \rightarrow \mathrm{SiO_2} + \mathrm{Si}$$

The phase separation of nanocrystalline Si from amorphous SiO_2 is revealed by the XRD measurement results shown in Figure 1. The appearance of wide diffraction peaks corresponding to (111), (220), and (311) planes of cubic silicon in pattern b evidences the growth of Si nanocrystallites from amorphous starting material, i.e., SiO powder, whose XRD pattern is shown as curve a for comparison. An average size of ~3.6 nm of the phase-separated Si crystallites is estimated from the widening diffraction peaks using the Scherrer formula. As a result of HF etching, SiO_2 phase has almost been dissolved and removed. The XRD pattern of etched sample (pattern c) is in absence of a wide diffraction peak at ~21° corresponding to amorphous SiO_2, indicating clearly the effect of HF etching. Pattern d represents the XRD of alkyl-terminated Si nanoparticles. The average size of Si particles after etching and alkyl-termination processes estimated from widening of diffraction peaks shows few changes. However, the surface composition has been modified distinctly by etching and thermal alkylation reaction, which is identified by the FTIR absorption spectra (Figure 2) of etched and surface-alkylated particles compared to the annealed and initial amorphous powders. Curves a−d show the FTIR spectra for amorphous SiO, annealed, HF-etched, and octene-treated sample, respectively. Before HF etching, there are only strong peaks at 1070−1100 cm^{-1} for SiO powders and the annealed sample, which can be assigned to Si−O vibration. The appearance of a strong peak at ~2100 cm^{-1} arising from Si−H_x stretching mode and 910 and 640 cm^{-1} from Si−H_x scissors mode in curve c indicates the Si−H terminated surfaces of particles. There are also peaks at 1080 cm^{-1} remaining in the HF-etched sample, indicating that some silicon atoms on particle surfaces still bind with

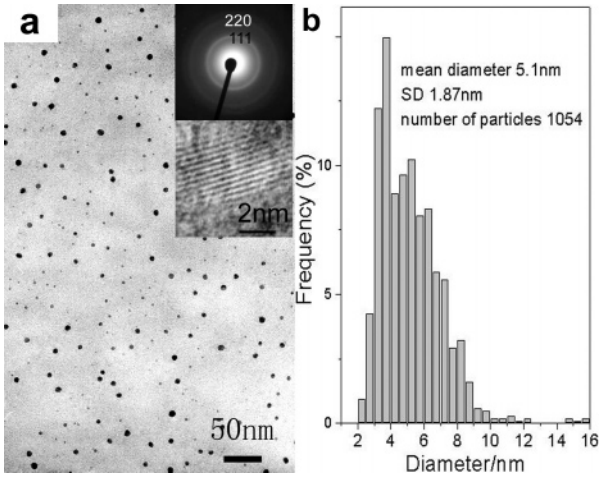

Figure 3. (a) TEM image of octene-treated sample with the SAED pattern and HRTEM image shown in the upper and lower inset, respectively. (b) Histogram of particle size distribution.

oxygen. The FTIR spectrum (curve d) of Si particles after reaction with octene shows strong bands for C−H stretching modes around 2900 cm^{-1} and weak bands for $\delta(CH_x)$ at ~1460 cm^{-1}; meanwhile, the obvious loss of the bands intensity for Si−H_x modes at 2100, 915, and 640 cm^{-1} as well as the absence of C═C stretching modes at 991 and 908 cm^{-1} indicate the formation of Si−C bond on the particle surfaces after the reaction between octene and Si−H surface, even though the band due to Si−C mode that should appear at ~1083 cm^{-1} is overlapped by that due to Si−O mode in curve d.

Figure 3a shows a typical micrograph of octyl-terminated Si nanoparticles, including a large number of well-dispersed particles. A selected area electron diffraction (SAED) pattern and high-resolution (HR) image with lattice fringes are shown in the upper and lower inset, respectively. The diffraction rings from inner to outer can be indexed as {111}, {220}, and {311} crystal planes of cubic silicon, respectively. The spacing of lattice fringes measured from the HR image is 0.30 nm, which is consistent with the *d* value of {111} planes (0.314 nm) of silicon. Both the SAED and the HR images confirm the high crystalline quality of the small particles. From Figure 3a and other images taken at different

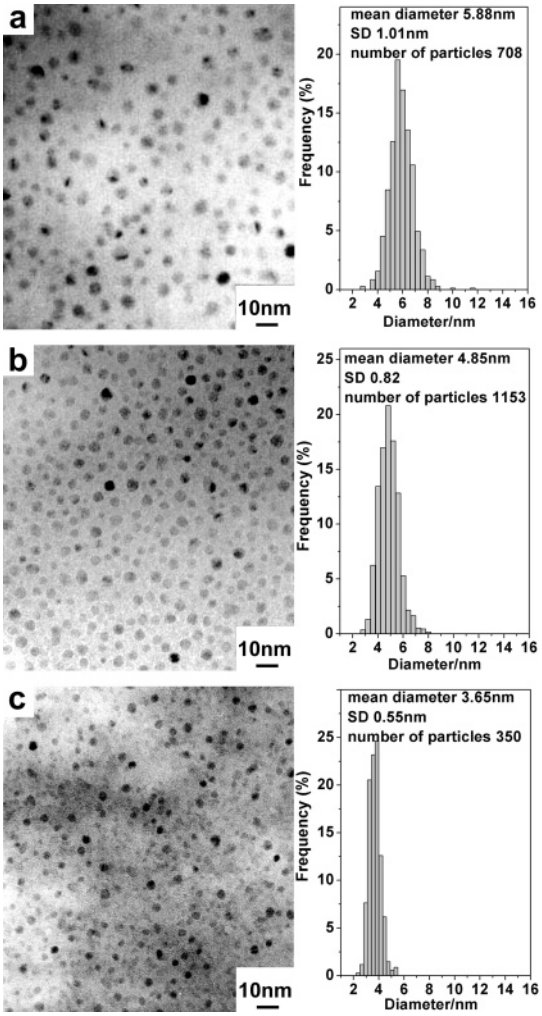

Figure 4. TEM images and corresponding histograms of size distribution of size-selected samples.

positions on the Cu grid the histogram of particle diameters shown in Figure 3b was generated by measuring approximately 1000 particles. It shows polydisperse particles ranging from 2 to 16 nm; thus, size classification techniques were adopted to narrow the size distribution.

It is known that size-selective precipitation has been extensively used for size classification of nanoparticle dispersions such as CdSe and CdS synthesized by a wet-chemical route. We performed size-selective precipitation for the polydisperse octyl-coated Si nanoparticle suspension using methanol as nonsolvent and usually we could obtain six to seven fractions. The average size of every fraction determined by TEM becomes smaller in the precipitation sequence. Figure 4 shows the TEM images and corresponding histograms of three representative fractions. Figure 4a corresponds to the first precipitate. Obviously, this fraction shows an increase in the average size and a decrease in the size distribution compared to what has been observed before size selection (Figure 3). The average particle size is 5.88, 4.85, and 3.65 nm for the three fractions, respectively. For the last two precipitates, in some cases, the TEM imaging contrast ratio was poor for those small Si particles as Si is a comparatively light element; thus, it is difficult to accurately measure the size distribution for the smaller particles present in these finally separated fractions. Anyway, the TEM results

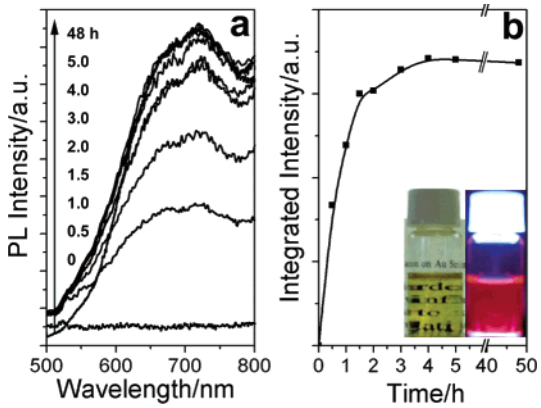

Figure 5. (a) Room-temperature photoluminescence spectra of the sample as a function of refluxing time during alkylation reaction. (b) The dependence of PL intensity on the refluxing time. Note that the final point on the curve indicates 48 h after the beginning of the reaction. The inset of (b) is the photograph of Si nanoparticle dispersion under a room lamp (yellow one with a paper printed by letters behind) and UV lamp (red one).

directly demonstrate that our octyl-capped Si nanoparticles of different average sizes can be separated from the organic dispersion by using the simple but effective method of size-selective precipitation.

Optical Properties. The influence of the alkyl termination on the PL properties has been investigated by several groups. Earlier studies on surface alkylation of PS or free-standing Si nanoparticles have indicated that the nature of the termination plays an important role in the PL intensity and stability of both PS and free-standing Si nanoparticles. It was noted that hydrosilylation of aliphatic olefins showed no decrease in PL intensity of PS compared to the initial $Si-H_x$ surfaces.[11] In other cases, however, the PL intensity of PS has been partly or significantly quenched on alkylation.[10,12,29−32] As for the alkyl/alkoxy-terminated free-standing Si nanoparticles prepared from reaction of $SiCl_4$ with Zintl salts, the UV−blue PL was remarkably stable for a period of 1 year,[21,22] while the visible PL of HF/HNO_3-etched Si nanoparticles was demonstrated to keep its initial intensity for months after surface coating by alkyl groups.[25] In this study, the evolution of PL emission with time during the alkylation reaction has been investigated, and significant enhancement of PL intensity has been found.

Figure 5 shows the PL spectrum of a typical sample, where emission at the wavelength longer than 800 nm cannot be detected due to the limit of our spectrometer. The sample was extracted at the given time intervals during refluxing and measured at the same condition. The amount of Si particles maintained constant so that the intensity of every spectrum is comparable. The spectrum at the bottom labeled as 0 h was measured on the dispersion before heating, thus representing the PL from hydrogen-passivated Si nanoparticles. It is seen that the PL intensity of the sample just after HF etching is very weak, mainly due to the large amount of nonradiative defects.[33] Our previous study[28] on Si nanopar-

(29) Song, J. H.; Sailor, M. J. *J. Am. Chem. Soc.* **1998**, *120*, 2376.
(30) Song, J. H.; Sailor, M. J. *Inorg. Chem.* **1999**, *38*, 1498.
(31) Sailor, M. J.; Lee, E. J. *Adv. Mater.* **1997**, *9*, 783.
(32) Kim, N. Y.; Laibinis, P. E. *J. Am. Chem. Soc.* **1998**, *120*, 4516.
(33) Murray, C. B.; Norris, D. J.; Bawendi, M. G. *J. Am. Chem. Soc.* **1993**, *115*, 8706.

ticles etched in various conditions demonstrate that complete H-passivated surface can be achieved by using diluted solution (~0.5%) of HF acid for more than 10 h. Only such well-passivated Si nanoparticles exhibit visible PL emission. In this study, we etched the annealed SiO powder using 10% HF solution for only 2 h and increased the product yield of the etched sample largely. As there is still some Si−O bonds besides the dominating Si−H ones, after this fast-etching process, the PL emission is very weak due to nonradiative defects on particle surfaces. However, as shown in Figure 5a, the relative PL intensity increases obviously from the beginning of refluxing, reaches a maximum after about 3 h, and then shows almost no changes even after 48 h. This is illustrated in Figure 5b, where the integrated PL (i.e., the area below the PL spectra shown in Figure 5a) is plotted versus the refluxing time. The refluxing period for reaching the maximum PL intensity differed from sample to sample, but within several hours further prolongation of refluxing time did not increase the PL intensity any more. In previous reports of other groups, alkylation reaction on PS samples was usually carried out for more than 10 h to achieve complete coating. Compared to the PS structure, the alkene molecules can attach the free-standing particle surfaces more easily, so the alkylation reaction in our case does not need such a long time.

A photograph taken under room light (yellow) and UV lamp (red) for the toluene dispersion of alkylated Si nanoparticles is shown in the inset of Figure 5b. It is seen that refluxing the Si particle in the presence of octene resulted in a transparent yellowish dispersion, through which letters on the paper placed behind the bottle can be seen clearly. The dispersion shows strong red emission under UV lamp irradiation. After the alkylated samples were stored in ambient air for 1 month, they were checked again. No significant changes were noticed. Hence, in this alkylation reaction, a large number of nonradiative defects have been effectively scavenged by refluxing at 110 °C and alkyl coating within several hours. Thus, both the dispersibility of nanoparticles in organic solvent and the emission intensity of the Si particles have been enhanced greatly in the current treatment. Herein, we suggest two effects of the alkylation reaction on the properties of Si nanoparticles. One is the derivatization of alkyl groups on particle surfaces, which contributes to the dispersibility of Si nanoparticles in nonpolar solvents. The other is the effective eliminantion of nonradiative defects on the particles, which results in enhanced PL emission. Murray et al. reported that annealing II−VI semiconductor nanocrystals in coordinating solvents provided high sample quality and resulted in strong band gap PL emission.[33] Thus, we consider that refluxing of our Si nanoparticle dispersion above 110 °C not only provides the thermal energy to the alkylation reaction but also anneals the sample so that well-passivated surfaces of highly crystalline nanoparticles can be achieved. As a consequence, our sample exhibits visible PL emission. It has also been noticed that the red emission band from the as-prepared alkyl-capped nanoparticle suspension is rather wide. We ascribe this band widening to the wide size distribution known from the corresponding TEM micrograph shown in Figure 3.

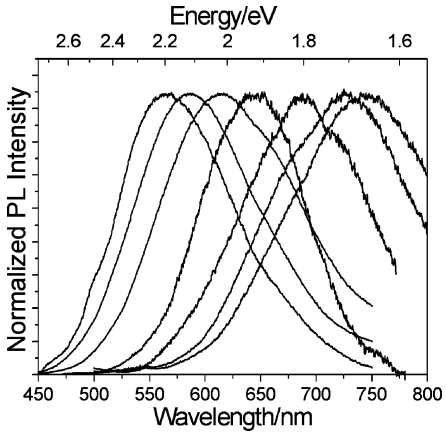

Figure 6. Room-temperature photoluminescence spectra of size-selected Si nanoparticles.

TEM results shown in Figure 4 have demonstrated the effectiveness of the size-selective precipitation technique. Herein, the room-temperature PL spectra shown in Figure 6 illustrate again the advantage of size-selective precipitation. Furthermore, the mechanism of PL emission is investigated by using those size-selected samples. Figure 6 clearly shows that tuning of the PL emission is possible by repeating the size-selective precipitation process. Usually Si nanoparticles at a size of ~6 nm and above in the first precipitate show emission wavelength longer than 800 nm that is out of the detection limit of our spectrometer. When the particle size was decreased from 6 to less than 3 nm, the PL peak energy shifted toward shorter wavelengths from 800 nm (1.55 eV) to 560 nm (2.19 eV). This obvious dependence of PL peak energies on nanoparticle sizes suggests that the optical luminescence of our samples is the result of quantum confinement effect; i.e., as the dimension of a semiconductor quantum structure decreases, the band gap of the material increases. This quantum effect has also been investigated theoretically.[34−38] Here, our experimentally observed emission bands will be compared to theoretical calculations of the exciton energy to demonstrate the quantum confinement effect in our Si nanoparticle.

According to the theoretical model of refs 35 and 38, the PL energy is blue-shifted with respect to the band gap of bulk silicon ($E_0 = 1.17$ eV) and obeys the following power law:

$$E_{\mathrm{PL}} = E_0 + \frac{3.73}{D^{1.39}} \tag{1}$$

This equation has been modified as eq 2:[38]

$$E_{\mathrm{PL}}^{\mathrm{corr}} = E_0 + \frac{3.73}{D^{1.39}} + \frac{0.881}{D} - 0.245 \tag{2}$$

The calculations of PL energy versus diameter of Si nanoparticles from eqs 1 and 2 are shown in Figure 7, in which the dotted and dashed curves correspond to eqs 1 and

(34) Takagahara, T.; Takeda, K. *Phys. Rev. B* **1992**, *46*, 15578.
(35) Delerue, C.; Allan, G.; Lannoo, M. *Phys. Rev. B* **1993**, *48*, 11024.
(36) Hill, N. A.; Whaley, K. B. *Phys. Rev. Lett.* **1995**, *75*, 1130.
(37) Datta, S.; Narasimhan, K. L. *Phys. Rev. B* **1999**, *60*, 8246.
(38) Ledoux, G.; Porterat, D.; Reynaud, C.; Huisken, F.; Kohn, B.; Paillard, V. *Phys. Rev. B* **2000**, *62*, 15942.

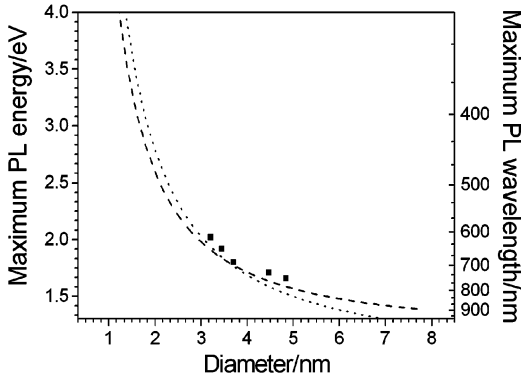

Figure 7. Photoluminescence peak energy of Si nanoparticles as a function of size. The solid squares are experimental data of this work, while the dotted and dashed lines represent the theoretical model of refs 35 and 38, respectively.

2, respectively. The solid squares represent PL peak energies measured from samples of our size-selected Si nanoparticles. As one can observe, the PL peak energies from our sample are consistent with the general trend of both theoretical curves. We have also noticed the small discrepancy between the experimental data and theoretical curve. It might come from two reasons. One is the accuracy of the small size determined by TEM observation. A previous report of Brus et al. on Si nanoparticles indicated that directly imaged Si nanocrystals in TEM are on the large side of the actual particle size distribution;[39] thus, the average size of every fraction of our sample determined by TEM measurements might be a bit larger than the actual one. On the other hand, Ledoux et al. found that PL yield increased as the size decreased and reached the maximum for 3 nm when they measured the PL yield of Si nanoparticles ranging from 2 to 8 nm.[40] In the present study, particle sizes are within the same range; therefore, particles on the small side of the distribution for every fraction contribute more to photoluminescence. As a result of both effects together, our experimental data are shifted a little to larger particle diameters or higher PL energies. However, the comparison between our experimental energies and the calculations still suggests that the emission we observed result from electron−hole recombination transitions in the Si nanocrystals due to quantum confinement effects if the small discrepancy is considered.

Conclusion

Both the dispersibility in nonpolar solvents and PL intensity of HF-etched Si nanoparticle sample are substantially enhanced by employment of the surface capping by octene. According to the experimental analyses, the thermal alkylation reaction enables remarkable reduction in nonradiative defects, which might produce PL emission due to radiative recombination of carriers confined in Si nanoparticles. Size-selective precipitation provided an effective means of tuning and narrowing the PL spectra. The band gap of the silicon nanoparticles could be shifted from 1.55 to 2.19 eV by decreasing the particle size. Our TEM measurements and PL results of the size-selected samples provided convincing evidence of a quantum confinement effect in the silicon nanoparticles. Moreover, the experimental dependence of PL peak energies on particle sizes follows the theoretical curves.

Acknowledgment. Financial support and granting of the postdoctoral fellowship (P03278, #15.03278) of this work from the Japan Society for Promotion of Science is gratefully acknowledged. This work is also supported in part by a Grant-in-Aid for Scientific Research (S: 16101003).

CM0519636

(39) Littau, K. A.; Szajowski, P. J.; Muller, A. J.; Kortan, A. R.; Brus, L. E. *J. Phys. Chem.* **1993**, *97*, 1224.

(40) Ledoux, G.; Gong, J.; Huisken, F.; Guillois, O.; Reynaud, C. *Appl. Phys. Lett.* **2002**, *80*, 4834.